JOURNAL OF VIROLOGY, Oct. 2007, p. 11054–11068 Vol. 81, No. 20
0022-538X/07/$08.00+0 doi:10.1128/JVI.01266-07

Severe Acute Respiratory Syndrome Coronavirus Gene 7 Products Contribute to Virus-Induced Apoptosis▽

Scott R. Schaecher,[1] Erin Touchette,[2] Jill Schriewer,[2] R. Mark Buller,[2] and Andrew Pekosz[1,3]*

Departments of Molecular Microbiology[1] and Pathology and Immunology,[3] Washington University in St. Louis School of Medicine, 660 S. Euclid Ave., Campus Box 8230, St. Louis, Missouri 63110, and Department of Molecular Microbiology and Immunology, St. Louis University Health Sciences Center, 1402 South Grand Blvd., St. Louis, Missouri 63104[2]

Received 11 June 2007/Accepted 20 July 2007

The proteins encoded by gene 7 of the severe acute respiratory syndrome coronavirus (SARS-CoV) have been demonstrated to have proapoptotic activity when expressed from cDNA but appear to be dispensable for virus replication. Recombinant SARS-CoVs bearing deletions in gene 7 were used to assess the contribution of gene 7 to virus replication and apoptosis in several transformed cell lines, as well as to replication and pathogenesis in golden Syrian hamsters. Deletion of gene 7 had no effect on SARS-CoV replication in transformed cell lines, nor did it alter the induction of early apoptosis markers such as annexin V binding and activation of caspase 3. However, viruses with gene 7 disruptions were not as efficient as wild-type virus in inducing DNA fragmentation, as judged by terminal deoxynucleotidyltransferase-mediated dUTP-biotin nick end labeling (TUNEL) staining, indicating that the gene 7 products do contribute to virus-induced apoptosis. Disruption of gene 7 did not affect virus replication or morbidity in golden Syrian hamsters, suggesting that the gene 7 products are not required for acute infection in vivo. The data indicate that open reading frames 7a and 7b contribute to but are not solely responsible for the apoptosis seen in SARS-CoV-infected cells.

Severe acute respiratory syndrome coronavirus (SARS-CoV) was first identified as the causative agent of a severe respiratory illness that affected more than 8,000 people worldwide during 2003 and 2004 (4). The pathogenesis of SARS-CoV infection has been well documented, with viral antigen detected predominantly in the respiratory alveolar epithelium but also in the intestinal epithelium, spleen, lymph nodes, liver, heart, renal distal tubule epithelium, central nervous system, and skeletal muscle (reviewed in references 21 and 35). Pathological evidence for both apoptosis and necrosis has been documented in various tissues obtained from SARS-CoV-infected humans (6, 14, 15, 26, 34).

SARS-CoV contains a positive-sense, single-stranded RNA genome of approximately 30 kb and utilizes a set of 3′-coterminal subgenomic RNAs (sgRNA) that are transcribed from the full-length single-stranded genome to facilitate viral protein expression (40, 55, 68). The genome contains open reading frames (ORFs) for eight accessory or group-specific proteins (ORF3a, -3b, -6, -7a, -7b, -8a, -8b, and -9b) with no clear homologues identified in other viruses of the *Nidoviridae*. Numerous studies have analyzed the in vitro expression of the SARS-CoV accessory proteins; however, the role that each accessory gene plays in virus infection is still unclear. Four of the accessory proteins, the ORF3a, ORF6, ORF7a, and ORF7b proteins, are thought to be packaged into viral particles (24, 25, 27, 57, 59), suggesting potential roles in entry, uncoating, or assembly.

Many SARS-CoV proteins induce apoptosis and/or necrosis when expressed from cDNA (10, 29, 30, 33, 36, 38, 63, 73, 76, 80, 84). The mechanisms for induction of cell death by the viral proteins are not clear, and it is unknown if these proapoptotic events play a significant role in induction of cell death during virus infection. In particular, the proteins encoded by SARS-CoV gene 7, the ORF7a and ORF7b proteins, not only induce apoptosis but inhibit cellular protein synthesis, activate the p38 mitogen-activated protein kinase (MAPK) signaling pathway, activate NF-κB, block cell cycle progression, and interact with the cellular transcription factor small glutamine-rich tetratricopeptide repeat-containing protein (SGT) as well as the antiapoptotic regulator Bcl-X_L (17, 28, 31, 67, 81). The relevance of these functions in context of viral infection is presently unknown.

Previous reports have demonstrated that recombinant SARS-CoV either containing a deletion of the gene 7 coding region or encoding green fluorescent protein (GFP) in place of the ORF7a and ORF7b proteins replicates with wild-type kinetics in transformed and primary cell cultures (60, 79) and in the lungs of BALB/c mice (79). These results suggest that ORF7a and ORF7b are dispensable for acute replication both in vitro and in vivo; however, a more detailed study of the deletion viruses is required to address potential roles for gene 7 proteins in the induction of cellular death and in altering other aspects of viral pathogenesis.

In this study, we provide a detailed analysis of the in vitro and in vivo replication kinetics of recombinant SARS-CoV strains with the gene 7 region deleted completely or replaced with GFP. The viruses replicated to similar infectious virus titers and with similar kinetics in Vero, CaLu-3, and CaCo-2 cells. The viruses induced similar levels of cell death; however, viruses carrying a disrupted gene 7 had significantly reduced numbers of terminal deoxynucleotidyltransferase-mediated dUTP-biotin nick end labeling (TUNEL)-positive, infected

* Corresponding author. Mailing address: W. Harry Feinstone Department of Molecular Microbiology and Immunology, Johns Hopkins University Bloomberg School of Public Health, 615 North Wolfe Street, Suite E5132, Baltimore, MD 21205. Phone: (410) 955-3223. Fax: (410) 955-0105. E-mail: apekosz@jhsph.edu.

▽ Published ahead of print on 8 August 2007.

cells but not activated caspase 3-or annexin V-positive cells, indicating a defect in the induction of DNA fragmentation. Virus replication in hamsters was not altered in the absence of gene 7. These results suggest that the gene 7 products specifically alter the virus-induced apoptotic pathway; however, acute virus replication is not altered by these changes.

MATERIALS AND METHODS

Cells. Vero (ATCC CRL-1586), CaLu-3 (ATCC HTB-55), and HEK-293T (64) cells were cultured in complete medium (Dulbecco's modified Eagle medium containing 10% fetal bovine serum [Atlanta Biologicals], 1 mM glutamine [Gibco], 1 mM sodium pyruvate [Cellgro], 100U/ml penicillin [Gibco], and 100 μg/ml streptomycin [Gibco]). CaCo-2 cells (ATCC HTB-37) were cultured in minimum essential medium (Eagle) with 2 mM L-glutamine and Earle's balanced salts solution adjusted to contain 1.5 g/liter sodium bicarbonate, 0.1 mM nonessential amino acids, 1.0 mM sodium pyruvate, and 20% fetal bovine serum. Cells were incubated in a 5% CO_2 humidified incubator at 37°C.

For cell death and apoptosis experiments, cells transfected with influenza virus M2 cDNA were incubated in medium containing 5.0 μM amantadine. Vero cells treated with brefeldin A (BFA) (Sigma) were incubated in complete medium containing 0.5 μg/ml BFA for the designated time periods to induce apoptosis (58).

Viruses. Recombinant SARS-CoVs were kindly provided by Ralph Baric, University of North Carolina. Briefly, nucleotides 27276 to 27643 (accession number A278741) were either deleted or replaced with the ORF for GFP, and recombinant viruses generated as previously described (60, 78, 79).

Recombinant SARS-CoV stocks were generated by infecting Vero cells with recombinant SARS-CoV at a multiplicity of infection (MOI) of 0.1, followed by incubation at 37°C for 48 h (44, 57). Infectious virus titers were determined by plaque assay or 50% tissue culture infectious dose ($TCID_{50}$) as described previously (57). Plaque diameters from 25 plaques visible in Vero cell monolayers stained with naphthol blue-black (Sigma) were measured using a micrometer (Scienceware).

Vero, CaLu-3, or CaCo-2 cells in 12-well or 96-well tissue culture dishes were incubated in 250 μl or 100 μl of medium, respectively, containing SARS-CoV at various MOIs for 1 h at 25°C on a rocker table. Medium was aspirated, cells were washed three times with phosphate-buffered saline (PBS), and 1.0 ml or 100 μl fresh medium was added. Cells were incubated for the designated time periods at 37°C, and supernatant was harvested for determination of virus titer. The cells were either lysed in 1% sodium dodecyl sulfate (SDS), trypsinized and then fixed with 2% paraformaldehyde in PBS, or treated as described below. All infections were performed in a biosafety level 3 laboratory using institution-approved procedures.

Influenza A/Udorn/72 virus infections were performed on Vero cells at an MOI of approximately 5.0 as described previously (41, 47). La Crosse virus (original strain) infections were also performed at an MOI of approximately 5.0 in complete medium (46).

Plasmids. Plasmids containing the coding sequences for SARS-CoV ORF7a, ORF7b, or influenza A virus M2 have been described previously (41, 42, 57).

Transient transfection of mammalian cells. The Lipofectamine 2000 transfection reagent (Invitrogen) was used according to the manufacturer's protocol for cells in suspension, using a reagent-to-DNA ratio of 3:1. Briefly, 1.0 μg of plasmid DNA was diluted into 50 μl of Opti-MEM medium (Gibco), and 3 μl of Lipofectamine 2000 reagent was added to another 50 μl of Opti-MEM. After 5 min of incubation at room temperature, the two suspensions were combined, vortexed, and incubated at room temperature for 20 min. Approximately 4×10^5 293T or Vero cells were centrifuged, resuspended in 400 μl Opti-MEM, and subsequently added to the DNA-liposome suspension. Cells were incubated at room temperature for 15 min and transferred into six-well tissue culture dishes (Corning), and an additional 500 μl Opti-MEM was added. Dishes were incubated at 37°C for 6 to 8 h. After incubation, transfection medium was aspirated and replaced with 2 ml complete medium, and cells were incubated at 37°C for the designated time periods.

IFA and confocal microscopy. For indirect immunofluorescence analysis (IFA), cells were stained and mounted as previously described (44, 57). The primary antibodies used were rabbit anti-ORF7b polyclonal serum (1:1,000) (57), anti-ORF7a mouse monoclonal antibody (MAb) 2E11 (1:1,000 dilution) (44), anti-GM130 mouse MAb (1:100 dilution; BD Biosciences), rabbit anti-calnexin immunoglobulin G (IgG) (1:100 dilution; Chemicon), and rabbit anti-ERGIC53 IgG (1:100 dilution; Sigma). Mitochondrial staining was performed using MitoTracker Red CMXRos (Invitrogen) at 250 nM per the manufacturer's protocol. Cells were washed three times with PBS, incubated with secondary antibody (goat anti-mouse IgG AlexaFluor 488, goat anti-mouse IgG AlexaFluor 555, goat anti-rabbit IgG AlexaFluor 488, or goat anti-rabbit IgG AlexaFluor 555, Molecular Probes) as appropriate (1:500 dilution). Nuclei were counterstained concurrently with TO-PRO-3 iodide (Invitrogen). Coverslips were mounted onto microscope slides using Prolong Antifade Gold (Molecular Probes) and visualized on a Zeiss LSM 510 META confocal microscope.

FACS. Fluorescence-activated cell sorting (FACS) was performed as described previously (44, 57). Cells were incubated with the anti-ORF7a murine MAb 2E11 (1:1,000 dilution) (44), anti-ORF7b rabbit serum (1:1,000 dilution) (57), anti-SARS S MAb cocktail (1:100 dilution; kindly provided by CDC), anti-SARS mouse hyperimmune serum (1:1,000 dilution; kindly provided by CDC), or anti-active caspase 3 rabbit MAb (1:1,000 dilution; R&D Systems) followed by goat anti-mouse IgG (1:500 dilution, AlexaFluor 488 or AlexaFluor 647 labeled; Molecular Probes) or goat anti-rabbit IgG (1:500 dilution, AlexaFluor 488 or AlexaFluor 647 labeled; Molecular Probes) secondary antibody. All antibody dilutions were made in blocking buffer. Wash buffer consisted of PBS with 0.1% saponin. The cells were analyzed with a FACSCalibur dual-laser flow cytometer (Becton Dickinson), and data were collected with CellQuest software.

ATP assay. The transfected cell suspensions were mixed 1:1 with complete medium and plated into 96-well black-walled assay dishes (Corning). For the analysis of virus-infected cells, Vero, CaLu-3, or CaCo-2 cells were plated in 96-well black-walled assay dishes infected at an MOI of approximately 5.0. At the indicated times posttransfection or postinfection, 100 μl CellTiter-GLO ATP assay reagent (Promega) was added to each well, and the plates were placed on a shaker table for 5 min. Plates were subsequently analyzed for luminescence on a Lumax luminometer (Molecular Technologies). Values at each time point were analyzed in sextuplet and graphed with standard deviations. The relative ATP concentration was calculated as a percentage of mean luminescence of pCAGGS empty vector-transfected cells.

TUNEL. For FACS analysis, transiently transfected or infected Vero cells were resuspended from 6- or 12-well tissue culture plates using trypsin-EDTA, washed three times with PBS, and fixed with 250 μl 1% methanol-free formaldehyde in PBS for 10 min at 25°C. After fixation, cells were washed twice with PBS. TUNEL staining was performed using either the fluorescein isothiocyanate (FITC)- or tetramethylrhodamine (TMR)-conjugated in situ cell death detection kit (Roche) per the manufacturer's protocol. The cells were analyzed with a FACSCalibur dual-laser flow cytometer (Becton Dickinson), and data were collected with CellQuest software. In dual-labeling experiments, the cells were immunostained for viral antigen or caspase 3 prior to TUNEL staining. Experiments under all conditions were performed in triplicate, and values were graphed with standard deviations.

For IFA, Vero cells were grown on glass coverslips in 12-well tissue culture plates. At approximately 100% confluence, cells were infected at an MOI of 5.0 and incubated for 24, 48, and 72 h. Infected cells were washed three times with PBS, fixed with 2% paraformaldehyde in PBS for 10 min, and then processed for IFA as previously described (44, 57), followed by TUNEL staining performed as described above, with staining solution added directly atop the coverslips. Coverslips were mounted onto microscope slides using Prolong Antifade Gold (Molecular Probes) and visualized on a Zeiss LSM 510 META confocal microscope. Three confocal images were acquired per coverslip using a 63× oil immersion lens and z slices of 2.0 μm. A total of nine images were taken per virus infection at each time point. More than 1,000 cells per condition were counted, and the percent TUNEL-positive cells was calculated.

Annexin V. Transiently transfected or infected Vero cells were washed with PBS and the detached cells pelleted by centrifugation at 500 × g for 10 min. The adherent cells were detached with trypsin-EDTA and washed three times with PBS. The two cell populations were pooled and analyzed for apoptosis by annexin V staining of phosphatidylserine using the annexin V-FITC/propidium iodide kit (BD Biosciences) per the manufacturer's protocol. Briefly, cells were resuspended in a solution of 100 μl 1× binding buffer plus 5 μl annexin V-FITC plus 5 μl propidium iodide solution. Cells were incubated at 25°C for 15 min, 400 μl binding buffer was added to transiently transfected cells, and FACS analysis was performed immediately. Infected cells were pelleted by centrifugation, and resuspended in 1% methanol-free formaldehyde diluted in binding buffer, and incubated for 10 min at 25°C. Cells were then centrifuged, resuspended in 500 μl binding buffer, and analyzed by FACS.

SDS-polyacrylamide gel electrophoresis and Western blotting. Infected cells were lysed in 1% SDS in water and mixed at a 1:1 ratio with 2× Laemmli SDS-polyacrylamide gel electrophoresis sample buffer. Samples were loaded onto 15% polyacrylamide gels (Mini Trans-Blot; Bio-Rad). Separated polypeptides were transferred onto polyvinylidene difluoride membranes (Immobilon-Q; Millipore) and blocked in PBS containing 0.3% Tween 20 and 5% nonfat dry

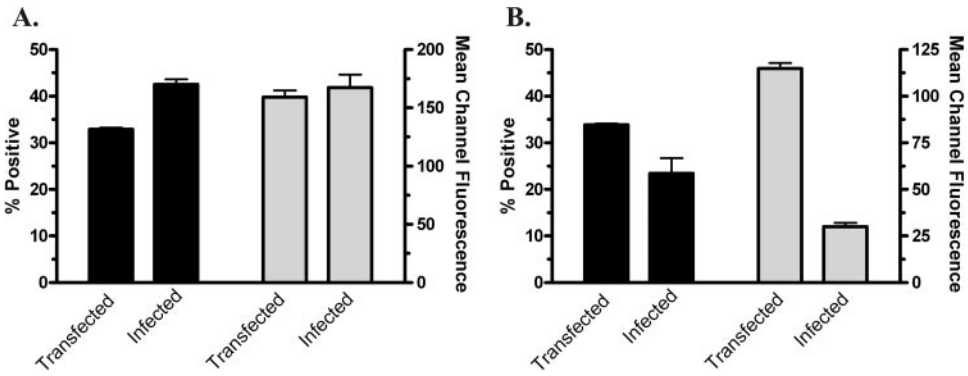

FIG. 1. Expression of the SARS-CoV accessory proteins ORF7a and ORF7b in cDNA-transfected and virus-infected cells. Vero cells were transfected with plasmids containing either the ORF7a or ORF7b cDNA and assayed for protein expression at 24 h posttransfection. Vero cells were infected with rSARS-CoV WT at an MOI of 5.0 and analyzed at 24 h postinfection. Flow cytometry was used to determine the percentage of cells expressing ORF7a (A) or ORF7b (B) and the relative protein expression levels (mean channel fluorescence). Data points are the averages for triplicate samples, and standard errors are shown.

milk (block buffer). Membranes were incubated with anti-β-actin mouse MAb (1:7,500 dilution; Abcam) and anti-active caspase 3 rabbit MAb (1:1,000 dilution; R&D Systems). Primary antibodies were detected using species-specific IgG secondary antibodies coupled to horseradish peroxidase (1:7,500 dilution; Jackson Laboratories). The blots were soaked in chemiluminescent reagent (ECL Plus Pico; Amersham Biosciences) and imaged using chemiluminescence and exposure to X-ray film (Molecular Technologies).

Infection of golden Syrian hamsters. Five- to 6-week-old golden Syrian hamsters (Charles River Laboratories) were housed three per cage in a biosafety level 3 animal facility. Animals were inoculated with PBS ($n = 6$) or 10^3 $TCID_{50}$ of either recombinant wild-type SARS-CoV (rSARS-CoV WT) ($n = 24$) or virus with GFP in place of the gene 7 coding region (rSARS-CoV GFPΔORF7ab) ($n = 24$) in a total volume of 100 μl (50 μl into each naris). Six saline-treated, 12 rSARS-CoV WT-infected, and 12 rSARS-CoV GFPΔORF7ab-infected animals were weighed at various times postinfection.

Three hamsters from each virus infection were sacrificed (56) on days 3, 5, 9, and 13 postinfection, and virus titers in homogenates of lung, kidney, liver, and spleen were determined. Tissues were weighed, complete medium was added to a achieve a 10% (wt/vol) suspension, and tissues were homogenized using tissue grinders (Fisher). After centrifugation at 3,400 rpm for 10 min, the supernatants were removed and analyzed by $TCID_{50}$ assay. All procedures were performed under protocols approved by the institutional biosafety and animal care committees.

RESULTS

Expression of SARS-CoV ORF7a and ORF7b in Vero cells. SARS-CoV sgRNA 7 encodes overlapping ORFs for two accessory proteins, ORF7a and ORF7b, and expression of both proteins has been confirmed experimentally in virus-infected cells (5, 9, 17, 18, 44, 57). Both the ORF7a and ORF7b proteins are single-pass integral membrane proteins, and both have been reported to be incorporated into viral particles (24, 44, 57). The translation initiation codon for ORF7a resides immediately proximal to the 5′ transcription regulatory sequence for sgRNA 7 and is predicted to be the predominant ORF translated from this sgRNA. The translation initiation codon for ORF7b resides 365 nucleotides from the transcription regulatory sequence and translation initiation occurs via ribosome leaky scanning, both of which serve to limit ORF7b translation (57).

To determine the relative expression levels of ORF7a and ORF7b when expressed from cDNA or in virus-infected cells, Vero cells were infected with SARS-CoV at an MOI of 5.0 or transiently transfected with plasmids encoding either ORF7a or ORF7b. Cells were harvested and fixed 24 h later and protein expression quantified using flow cytometry. ORF7a was detected in 32.9% ± 0.6% of the transfected cell population and in 42.5% ± 2.0% of the infected cell population (Fig. 1A). The relative protein expression levels in the two ORF7a-expressing cell populations were comparable (mean channel fluorescences of 159.1 ± 9.9 and 167.4 ± 19.5, respectively), indicating that transient transfection results in physiologically relevant levels of ORF7a protein expression. The ORF7b protein was detected in 33.9% ± 0.4% of transfected cells and 23.5% ± 5.6% of infected cells (Fig. 1B). Not surprisingly, the mean channel fluorescence was higher in cDNA-transfected cells (114.9 ± 5.1 compared to 30.0 ± 3.5), indicating that transient transfection of ORF7b results in significantly higher levels of protein expression than are normally observed in SARS-CoV-infected cells.

The ORF7b protein localizes to the Golgi apparatus in cDNA-transfected and virus-infected cells (57), but the ORF7a protein has been localized to the Golgi complex (31, 44, 49), to the endoplasmic reticulum (ER) and ER-Golgi intermediate compartment (18), and to mitochondria (67). When expressed from cDNA, neither ORF7a nor ORF7b colocalized with MitoTracker dye, particularly compared to high degree of colocalization seen with GM130, a marker of the *cis*-Golgi (Fig. 2). Some MitoTracker-positive organelles are adjacent to ORF7a- and ORF7b-positive membranes; however, it is clear that the vast majority of the signals do not overlap. A similar pattern was seen in SARS-CoV-infected cells (data not shown). Therefore, we conclude that the ORF7a and ORF7b proteins reside primarily if not exclusively in the Golgi complex when expressed from cDNA or in virus-infected cells.

Cells expressing the ORF7a or ORF7b protein undergo apoptosis. It has been reported that ORF7a and ORF7b induce apoptosis when expressed from cDNA (31, 66, 67). To confirm and extend those observations, Vero cells were transfected with plasmids expressing the cDNAs for ORF7a, ORF7b, or the influenza A virus M2 protein and then screened for the induction of cell death by multiple assays. Transfection efficiency was determined by flow cytometry at 24 h posttransfection (Fig. 3A). The ORF7a, ORF7b, and M2 proteins were

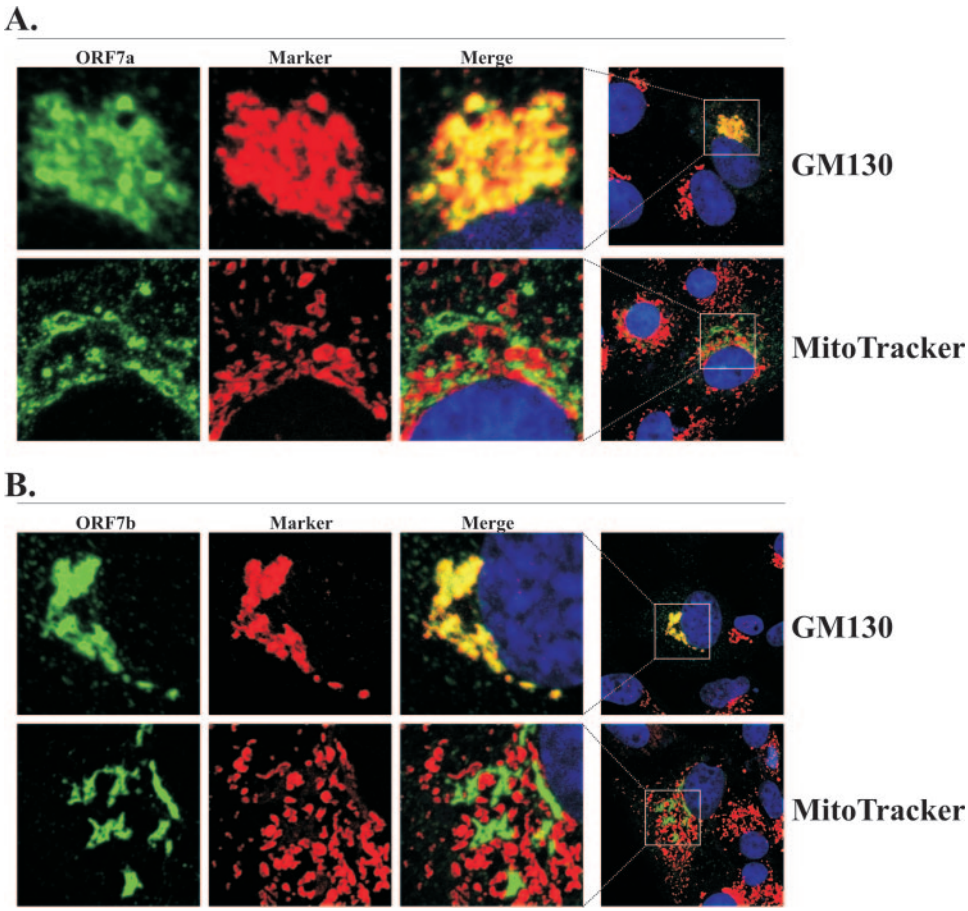

FIG. 2. The SARS-CoV ORF7a and ORF7b proteins localize to the Golgi apparatus. Vero cells grown on coverslips were transfected with plasmids expressing either ORF7a (A) or ORF7b (B) cDNA. At 18 h posttransfection, the cells were assessed by confocal microscopy for colocalization with either the *cis*-Golgi network (GM130) or mitochondria (MitoTracker), shown in red. Images were magnified to emphasize colocalization with GM130 and lack of colocalization with mitochondria. All images were obtained with a 63× oil immersion objective lens and represent a *z* stack projection of 0.5-μm optical slices.

expressed in 34.1% ± 0.5%, 27.13% ± 0.4%, and 26.8% ± 0.3% of cells, respectively. Next we assessed the effects of protein expression on cell viability by determining the relative amounts of ATP present in cells (Fig. 3B). The relative luminescence of ORF7a- and ORF7b-expressing cells was decreased by 11.8% ± 1.1% and 7.2% ± 1.0%, respectively, compared to empty vector-transfected cells. Expression of the M2 protein had little effect on cell viability, indicating that the reduced cell viability was specific to cells expressing either ORF7a or ORF7b and not a result of the expression of any viral protein. BFA treatment resulted in nearly complete cell death. These results demonstrate that expression of either ORF7a or ORF7b alone results in decreased cell viability.

To assess the contribution of apoptosis to the reduced viability of cells expressing ORF7a or ORF7b, we used three distinct assays that assess different aspects of apoptotic cell death. The presence of proteolytically activated caspase 3 is a hallmark of both the intrinsic and extrinsic apoptosis pathways (Fig. 3C). Active caspase 3 was detected in only 3.3% ± 0.1% and 3.2% ± 0.4% of empty vector- and M2 cDNA-transfected cells, respectively. However, significantly more ORF7a and ORF7b cDNA-transfected cells were active caspase 3 positive (16.9% ± 0.6% and 18.3% ± 0.8%, respectively). Treatment with BFA, a known inducer of apoptosis, resulted in 52.75% ± 1.5% active caspase 3-positive cells. Taken together, the data indicate that the expression of ORF7a or ORF7b leads to a modest but significant increase in activated caspase 3.

Another phenotypic change observed in apoptotic cells is the internucleosomal cleavage of chromosomal DNA, which can be detected with the TUNEL assay (Fig. 3D). Fragmented DNA was detected in 2.7% ± 0.5% and 3.3% ± 0.2% of empty vector- and M2 cDNA-transfected cells, respectively. ORF7a and ORF7b expression led to increased numbers of TUNEL-positive cells (8.9% ± 1.4% and 7.1% ± 1.0%, respectively), while BFA-treated cells were 59.4% ± 6.9% TUNEL positive. Again, the data support a modest but significant increase in apoptotic cells after the expression of ORF7a or ORF7b.

Finally, the amount of phosphatidylserine in the outer leaflet of the plasma membrane was quantified using annexin V binding and flow cytometry (Fig. 3E). Annexin V bound to 3.5% ± 0.4% and 5.9% ± 2.1% of empty vector- and M2-transfected cells, respectively. ORF7a and ORF7b expression led to an increase in the number of cells binding annexin V (12.4% ± 1.4% and 10.5% ± 1.3%, respectively). Again, BFA-treated

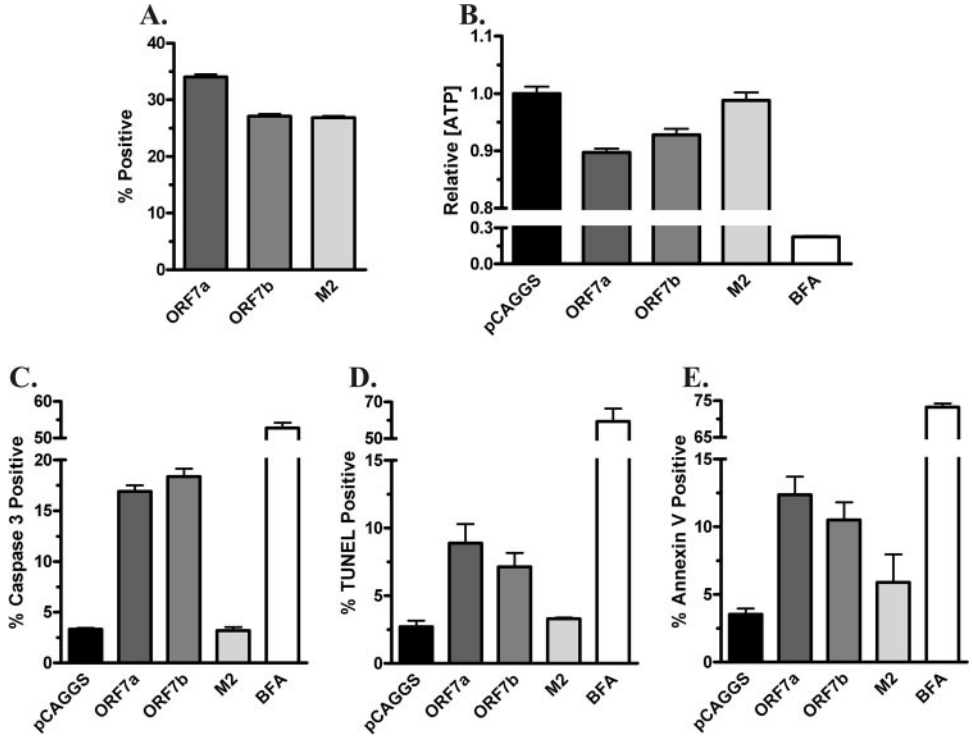

FIG. 3. Transient expression of ORF7a or ORF7b induces cell death by apoptosis in Vero cells. Vero cells were transfected with empty vector (pCAGGS) or plasmids encoding the SARS-CoV ORF7a, SARS-CoV ORF7b, or influenza A virus M2 cDNA and analyzed at 48 h posttransfection. Vero cells were incubated with 0.5 μg/ml BFA for 48 h. (A) The percentage of cells expressing the indicated protein was determined by flow cytometry. Data points are the averages for triplicate samples, and standard errors are shown. (B to E) Transfected cells were utilized for subsequent experiments at 48 h posttransfection. (B) The relative ATP content of Vero cells at 48 h posttransfection was analyzed to determine overall cell viability. Samples were analyzed in sextuplet; means and standard errors are shown. (C) Vero cells were analyzed for the presence of active caspase 3 using flow cytometry. Data points are the averages for triplicate samples, and standard errors are shown. (D) Vero cells were analyzed for the presence of fragmented DNA by TUNEL assay followed by flow cytometry. Data points are the averages for triplicate samples, and standard errors are shown. (E) Vero cells were analyzed for the presence of phosphatidylserine on the outer leaflet of the plasma membrane by annexin V-FITC staining followed by flow cytometry. Data points are the averages for triplicate samples, and standard errors are shown.

cells showed a significantly higher level of annexin V binding (73.3% ± 1.0%). Taken together, these results demonstrate that expression of ORF7a or ORF7b in Vero cells leads to a moderate increase in apoptotic cell death that is not seen after expression of other viral proteins from the same expression plasmid.

In vitro replication of SARS-CoV lacking gene 7. The data on the effects of SARS-CoV gene 7 proteins on host cell viability led us to investigate the contribution of these proteins to virus replication and cell killing. rSARS-CoV WT or viruses with either GFP in place of the gene 7 coding region (rSARS-CoV GFPΔORF7ab) (Fig. 4A) or a deletion of the gene 7 coding region (rSARS-CoV ΔORF7ab) were compared with respect to in vitro replication and induction of apoptosis. Cells infected with rSARS-CoV WT expressed high levels of the S, ORF7a, and ORF7b proteins (Fig. 4B). Compared to rSARS-CoV WT-infected cells, the rSARS-CoV GFPΔORF7ab-infected cells had similar amounts of S protein but no detectable ORF7a or ORF7b. There was, however, a strong fluorescence signal consistent with the expression of GFP in the cells.

Cytopathic effect induced by the viruses was analyzed by plaque assay. Vero cell monolayers infected with either virus were stained at 96 h postinfection with naphthol blue-black to visualize virus-induced plaques (Fig. 4C). Both viruses were able to form clear, distinct plaques in Vero cell monolayers, with nearly identical mean plaque diameters (4.61 ± 0.09 mm and 4.62 ± 0.07 mm for rSARS-CoV WT and rSARS-CoV GFPΔORF7ab, respectively), indicating that the gene 7 products did not alter plaque formation. Similar results were obtained with rSARS-CoV ΔORF7ab (data not shown).

The replication of recombinant wild-type and gene 7-deleted SARS-CoV was analyzed in single- and multistep growth assays on three different cell lines: Vero African green monkey kidney cells (Fig. 5A and B and 6A and B), CaLu-3 human lung adenocarcinoma cells (Fig. 5C and D and 6C and D), or CaCo-2 human colorectal carcinoma cells (Fig. 5E and F and 6E and F). The cells were infected with rSARS-CoV WT and rSARS-CoV GFPΔORF7ab at low (0.01) or high (5.0) MOI, infectious virus titers in the supernatants were determined by $TCID_{50}$ assay at various times postinfection (Fig. 5), and antigen spread in the cell monolayer was assayed by flow cytometry (Fig. 6). Consistent with previous reports (60), the viruses displayed similar patterns of replication, virus titer, and kinetics of antigen spread within each cell type, suggesting that gene 7 is not required for efficient virus replication in tissue culture. The growth kinetics for these viruses were similar to those observed with the SARS-CoV Urbani clinical isolate (data not shown). Identical results were obtained with rSARS-CoV

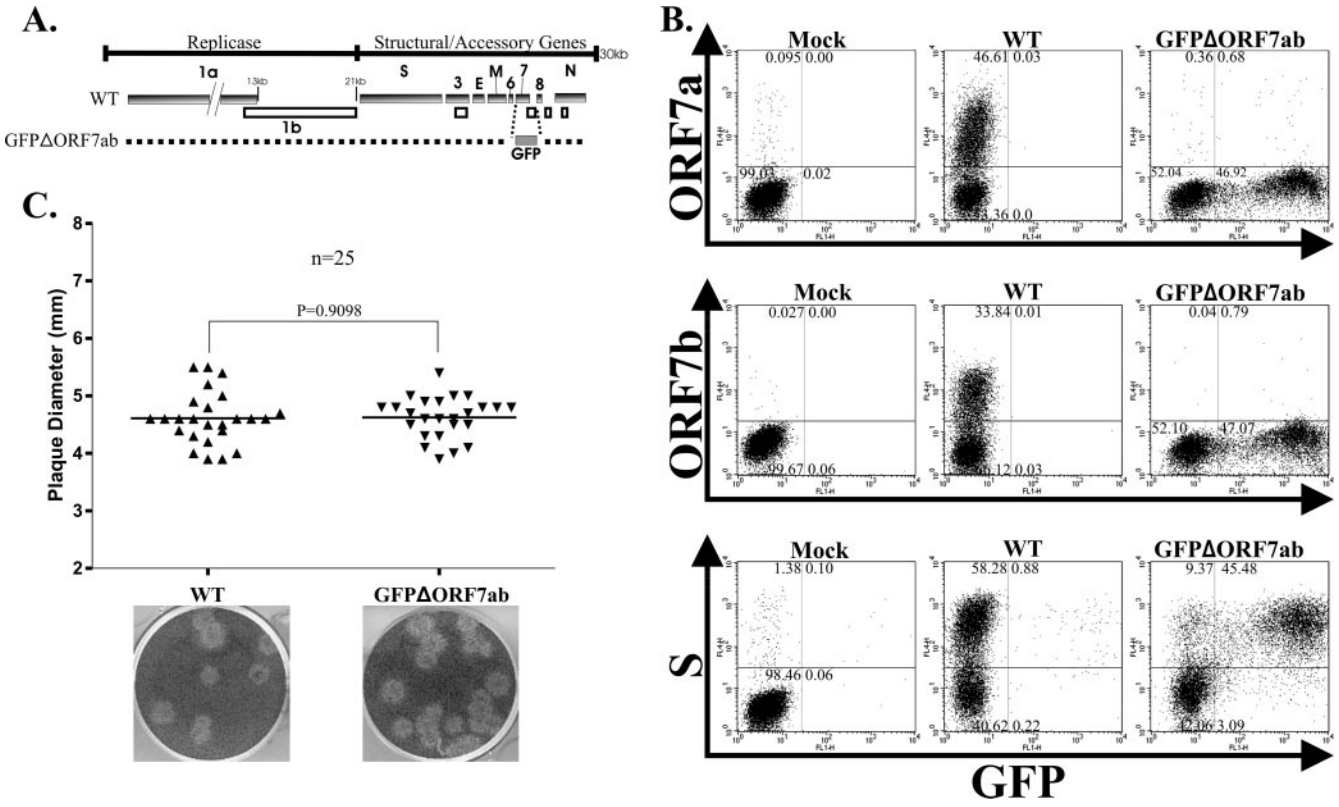

FIG. 4. Recombinant SARS-CoV containing GFP in place of ORF7a and ORF7b has normal plaque morphology. (A) Genomic organization of rSARS-CoV WT and rSARS-CoV GFPΔORF7ab. Genes carried by the viruses are indicated; open boxes represent downstream ORFs identified or predicted in bicistronic genes. The rSARS-CoV GFPΔORF7ab genome is identical to that of rSARS-CoV WT except that gene 7 has been replaced with the GFP gene. (B) Vero cells were either mock infected or infected with rSARS-CoV WT or rSARS-CoV GFPΔORF7ab at an MOI of 5. At 24 h postinfection, the cells were fixed and analyzed by flow cytometry for expression of ORF7a, ORF7b, S, or GFP. The percentage of cells in each quadrant is displayed. (C) Plaque assay with rSARS-CoV WT or rSARS-CoV GFPΔORF7ab on Vero cells. Plaque size was measured using a micrometer. Data represent diameter measurements of 25 plaques for each virus. The solid horizontal line is the average diameter; 95% confidence statistical significance was determined by a two-tailed paired *t* test. Representative images of infected tissue culture plates are shown.

ΔORF7ab (Fig. 5G and H and 6G and H). Taken together, the data indicate that there is no detrimental effect of deleting or replacing the SARS-CoV gene 7 on virus replication in transformed cell lines.

Induction of cell death by rSARS-CoV. The deletion of gene 7 did not alter the plaque-forming ability or replication of rSARS-CoV in transformed cell lines. We utilized an ATP cell viability assay in order to directly measure the effects of gene 7 deletion on SARS-CoV cell killing. Vero (Fig. 7A), CaLu-3 (Fig. 7B), and CaCo-2 (Fig. 7C) cells were infected with rSARS-CoV WT or rSARS-CoV GFPΔORF7ab at an MOI of approximately 5.0 and analyzed for total cell viability at various times postinfection. Both viruses induced cell death in Vero and CaLu-3 cells with similar kinetics and to similar extents as judged by relative ATP concentrations. Little or no cell death was observed in CaCo-2 cells with either virus, in agreement with previously described results (75). Infection of Vero cells with La Crosse virus and of CaLu-3 and CaCo-2 cells with influenza A virus (48, 65) resulted in rapid loss of cell viability. These findings indicated that infection of cells with rSARS-CoV GFPΔORF7ab results in similar levels of cell death as infection with wild-type virus.

Apoptosis induction by rSARS-CoV. Apoptosis can be divided into multiple stages (reviewed in reference 70). To address the induction of apoptosis by rSARS-CoV WT and gene 7 deletion viruses, we initially analyzed the activation of caspase 3 by flow cytometry and Western blotting. Vero cells were infected with either rSARS-CoV WT or rSARS-CoV GFPΔORF7ab at an MOI of approximately 5.0. At various times postinfection, cells were harvested and immunostained for active caspase 3 (Fig. 8A). Infection of Vero cells with both viruses resulted in activation of caspase 3 as early as 24 h postinfection, with the highest proportion of cells containing activated caspase 3 at 72 h. Lack of ORF7a and ORF7b had no deleterious effect on activation of caspase 3. Caspase 3 activation was confirmed by Western blotting at 72 h postinfection (Fig. 8A, inset), with little or no difference in signal intensity seen between virus-infected cells. To ensure that GFP expressed by the gene 7 replacement virus was not activating caspase 3 and masking a reduction in apoptosis activation, we analyzed caspase 3 activation by rSARS-CoV ΔORF7ab, which does not express GFP (Fig. 8B). As observed with the GFP replacement virus, infection of Vero cells with rSARS-CoV ΔORF7ab resulted in no change in activated caspase 3 com-

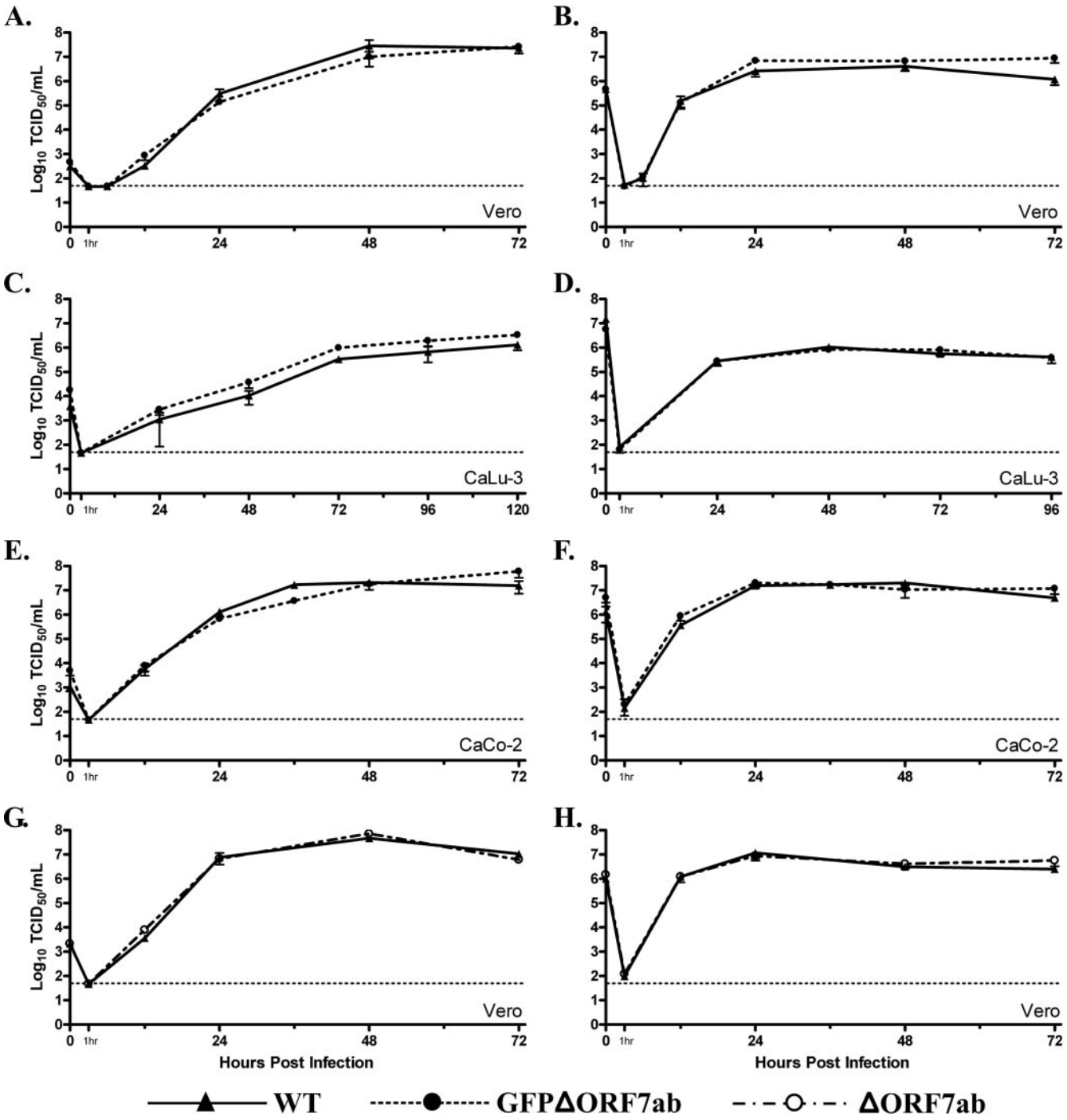

FIG. 5. Gene 7 deletion viruses have no replication defect in one- or multiple-step growth curves compared to rSARS-CoV WT on multiple cell types. Vero-E6, CaLu-3, and CaCo-2 cells were infected with rSARS-CoV WT (A to H), rSARS-CoV GFPΔORF7ab (A to F), or rSARS-CoV ΔORF7ab (G and H) at an MOI of 0.01 (A, C, E, and G) or 5.0 (B, D, F, and H). Media were collected at the designated time points and infectious virus titers determined by $TCID_{50}$. Data points are the averages for triplicate samples, and standard errors are shown.

pared to rSARS-CoV WT-infected cells. Double staining of cells for SARS-CoV antigen demonstrated that the active caspase 3 cell populations were predominantly positive for SARS-CoV antigen (data not shown), suggesting that the apoptosis was induced by virus infection and not through a bystander effect.

Next, the presence of phosphatidylserine in the outer leaflet of the plasma membrane, another marker for early stages of apoptosis, was quantified with FITC-labeled annexin V. Vero cells infected with rSARS-CoV WT or rSARS-CoV ΔORF7ab showed similar levels of annexin V binding at various times postinfection (Fig. 8C), again demonstrating that rSARS-CoV

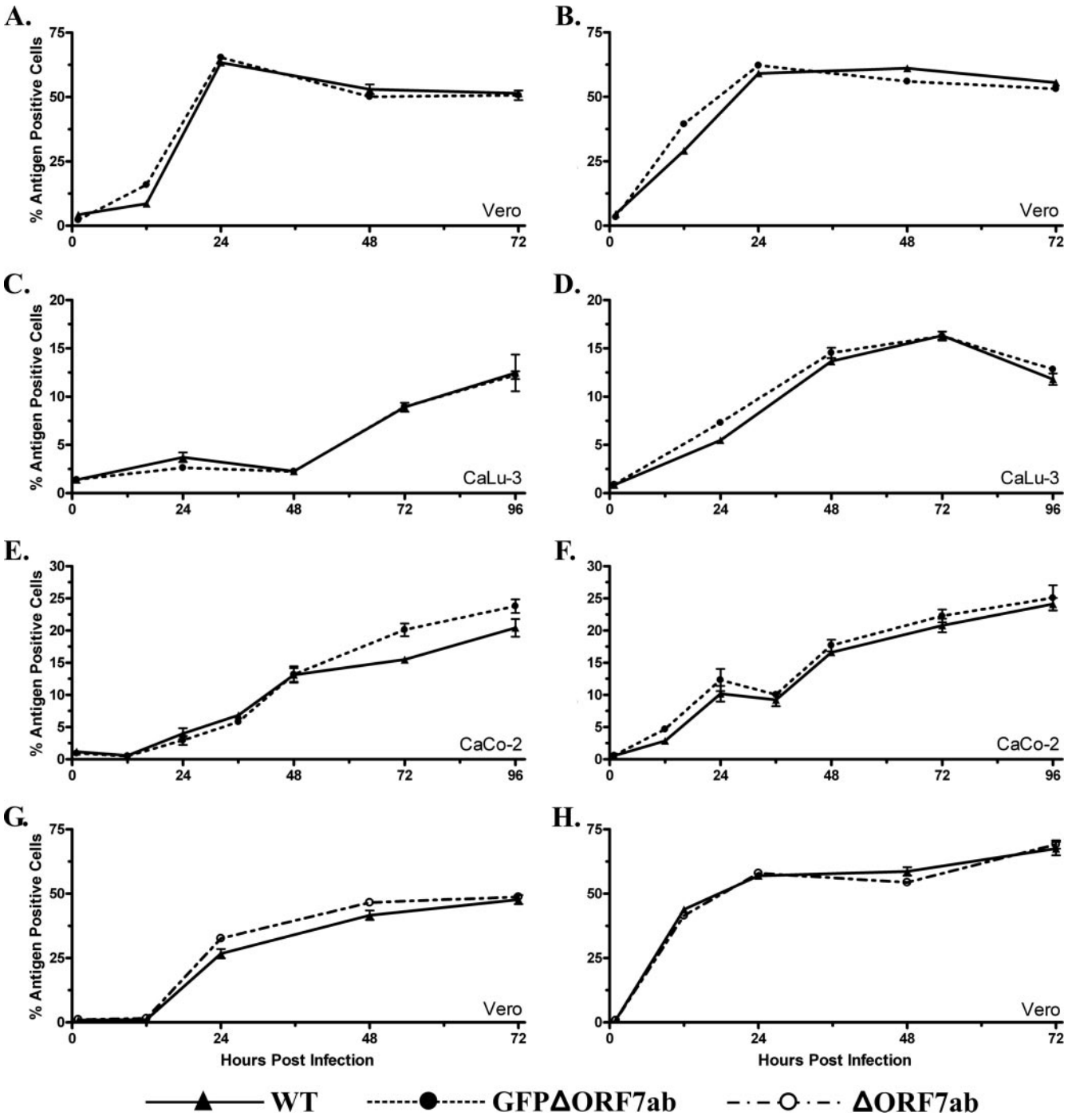

FIG. 6. SARS-CoV gene 7 does not alter infection or virus spread in multiple cell types. Vero-E6, CaLu-3, and CaCo-2 cells were infected with rSARS-CoV WT (A to H), rSARS-CoV GFPΔORF7ab (A to F), or rSARS-CoV ΔORF7ab (G and H) at an MOI of 0.01 (A, C, E, and G) or 5.0 (B, D, F, and H). At the designated times, the cells were collected and analyzed for SARS-CoV antigen by flow cytometry. Cells were immunostained with a mouse anti-SARS-CoV hyperimmune serum, and the percentage of SARS-CoV antigen-positive cells was quantified. The spread of viruses bearing alterations in gene 7 was nearly indistinguishable from that rSARS-CoV WT on all cell types tested. Data points are the averages for triplicate samples, and standard errors are shown.

ΔORF7ab induces early stages of apoptosis to levels equivalent to those seen with wild-type virus.

SARS-CoV lacking gene 7 is deficient in inducing DNA cleavage. To further address the programmed cell death cascade in virus-infected cells, Vero cells infected with either wild-type or gene 7 deletion viruses were analyzed for DNA fragmentation, a late event in apoptosis (11, 51), by TUNEL. Vero cells were infected with rSARS-CoV WT or rSARS-CoV ΔORF7ab at an MOI of approximately 5.0. Cells were harvested at various times postinfection, labeled by TUNEL assay,

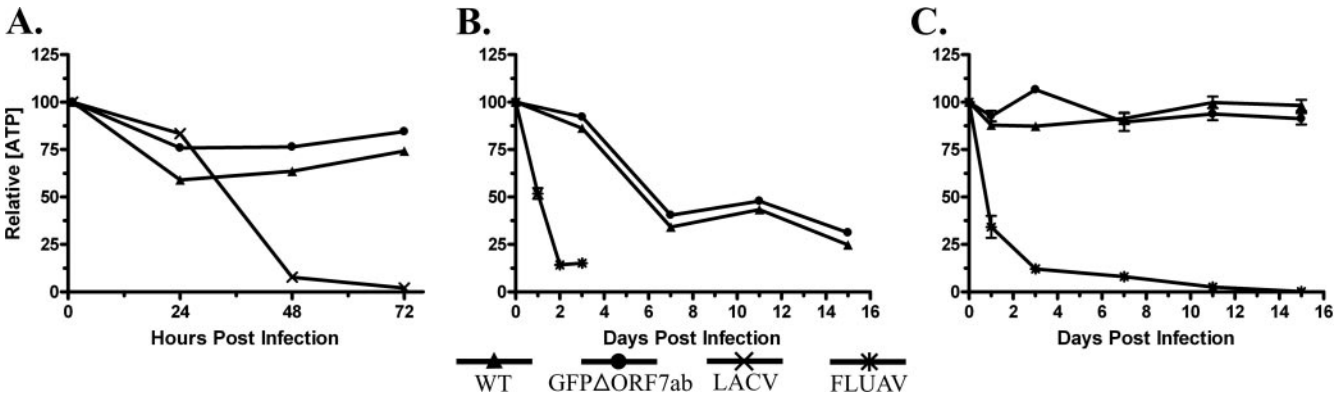

FIG. 7. The SARS-CoV gene 7 does not alter the cell-killing activity of the virus. (A) Vero, (B) CaLu-3, or (C) CaCo-2 cells were infected with rSARS-CoV WT, rSARS-CoV GFPΔORF7ab, influenza A virus (FLUAV), or La Crosse (LACV) virus at an MOI of approximately 5.0 in 96-well plates. At the designated times postinfection, total cell viability was analyzed by ATP assay.

and analyzed by flow cytometry (Fig. 9A). A significantly lower TUNEL-positive population was detected in cells infected with rSARS-CoV ΔORF7ab than in those infected with rSARS-CoV WT at 48 h (8.8% ± 0.3% and 22.0% ± 1.1, respectively) and 72 h (23.5% ± 1.9% and 68.6% ± 1.9%, respectively) postinfection.

The dichotomy observed between TUNEL-positive and active caspase 3-positive cell populations in rSARS-CoV ΔORF7ab-infected cells suggests that the induction of apoptosis by the gene 7 deletion viruses may differ from that observed in wild-type virus infection. To address the ratio of active caspase 3- to TUNEL-positive infected cell populations, flow cytometry was utilized to double stain infected cells for DNA fragmentation and activated caspase 3 (Fig. 9B). Cells were either mock treated or infected with rSARS-CoV WT or rSARS-CoV ΔORF7ab and harvested at various times postinfection. The results again indicate that a significantly higher number of cells infected with wild-type virus undergo DNA fragmentation than cells infected with rSARS-CoV ΔORF7ab; however, both viruses induce similar levels of active caspase 3. Interestingly, rSARS-CoV WT-infected cells at 72 h postinfection yielded nearly equal cell populations that were either double positive for active caspase 3 and TUNEL staining or were only singly positive for TUNEL staining. It is likely that the TUNEL single-positive cell population is in late stages of apoptosis and may no longer have detectable levels of active caspase 3.

To confirm the lack of DNA fragmentation, we repeated the TUNEL analysis with both gene 7 deletion and GFP replacement viruses using confocal microscopy. Vero cells grown on glass coverslips were infected with rSARS-CoV WT, rSARS-CoV ΔORF7ab, or rSARS-CoV GFPΔORF7ab and analyzed by immunofluorescence confocal microscopy at various times postinfection (Fig. 9C and D). Cells were stained for SARS-CoV antigen and TUNEL labeled, and nuclei were counterstained with TO-PRO-3 to highlight the nuclear architecture. Quantification of adherent TUNEL-positive cells confirms that both viruses lacking gene 7 had significantly fewer TUNEL-positive cells than cells infected with wild-type virus (Fig. 9C). The few TUNEL-positive cells in the gene 7 deletion virus-infected cells displayed the nuclear morphological changes and pyknosis associated with apoptosis observed in cells infected with wild-type virus (Fig. 9D). Taken together, these results indicate that recombinant SARS-CoV with gene 7 deletions replicates and induces early stages of apoptosis at levels comparable to those for wild-type virus in tissue culture. However, the induction of late stages of apoptosis, specifically DNA fragmentation, is significantly reduced.

Recombinant SARS-CoV lacking gene 7 replicates to wild-type levels in lungs of golden Syrian hamsters. Golden Syrian hamsters are among the best small animal models for analyzing SARS-CoV replication in vivo (53). Hamsters were inoculated with either 100 μl PBS or 10^3 $TCID_{50}$ of either rSARS-CoV WT or rSARS-CoV GFPΔORF7ab. Hamsters infected with either virus had slower weight gain than the control animals, indicating that the virus infection was inducing some morbidity (Fig. 10A). However, deletion of gene 7 did not drastically alter virus-induced morbidity (Fig. 10A). At the indicated days postinfection, lung, kidney, spleen, and liver tissues were harvested and analyzed for virus titer by $TCID_{50}$ assay. Virus was detectable at similar titers in the lungs of hamsters infected with either virus on days 2 and 5 postinfection (Fig. 10B) and was cleared from the lungs after day 5. Virus was not detectable by $TCID_{50}$ assay in any other tissues at any time point analyzed (data not shown). These data demonstrate that gene 7 products are not required for acute viral replication or overall morbidity in hamsters.

DISCUSSION

Various coronavirus accessory genes have been implicated as having important roles in virus replication and pathogenesis in vivo (13, 45); however, none of the SARS-CoV accessory genes are required for replication in tissue culture or in BALB/c mice (79). Few nucleotide polymorphisms exist within the ORF7a and ORF7b coding regions in the approximately 130 sequenced SARS-CoV isolates, suggesting the presence of a selective pressure to maintain gene 7. Both ORF7a and ORF7b coding regions are also highly conserved in all eight sequenced bat coronavirus isolates. Serial passage of SARS-CoV in Vero cells resulted in a 29-nucleotide deletion within ORF7b (68), suggesting that the protein is dispensable in vitro

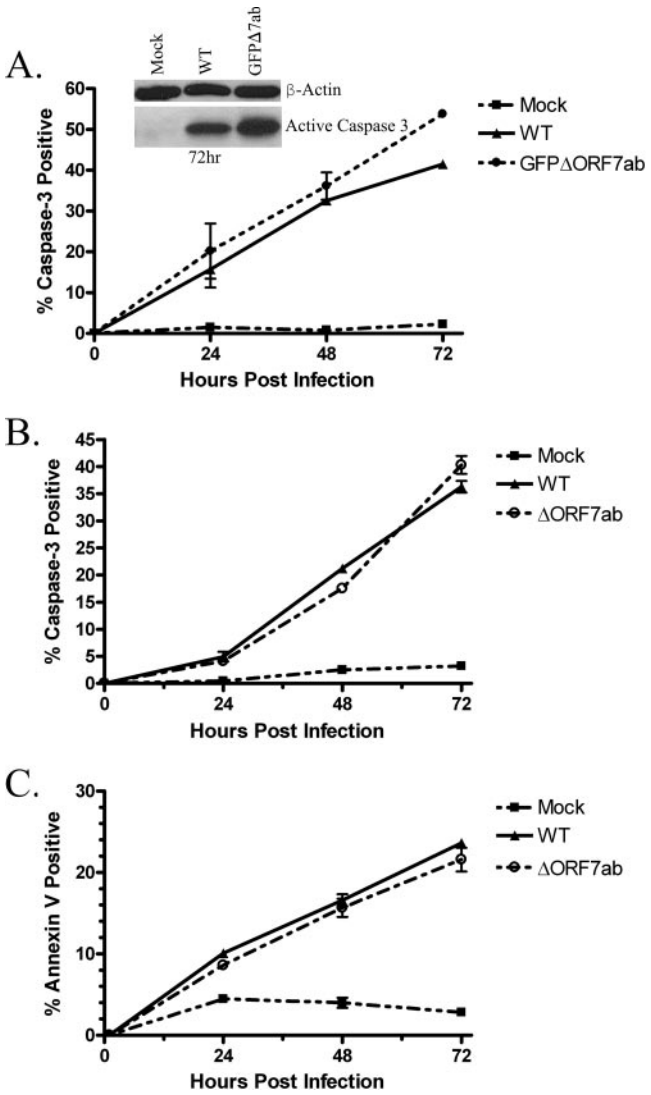

FIG. 8. The SARS-CoV gene 7 does not alter the induction of early- and middle-stage apoptosis. (A) Vero cells were mock infected or infected at an MOI of 5.0 with rSARS-CoV WT or rSARS-CoV GFPΔORF7ab, and cells were analyzed for active caspase 3 by flow cytometry. Caspase 3 activation was also analyzed by Western blotting (inset) at 72 h, with both viruses inducing similar levels of active caspase 3. Mock-infected cells contained little or no detectable active caspase 3 at all time points. Data points are the averages for triplicate samples, and standard errors are shown. (B) Vero cells were infected with rSARS-CoV WT or rSARS-CoV ΔORF7ab and analyzed for caspase 3 activation by flow cytometry. Data points are the averages for triplicate samples, and standard errors are shown. (C) Vero cells were infected with rSARS-CoV WT or rSARS-CoV ΔORF7ab and analyzed for apoptosis using annexin V-FITC staining and flow cytometry. Infection of both viruses resulted in nearly identical annexin V staining cell populations at 24, 48, and 72 h postinfection. Data points are the averages for triplicate samples, and standard errors are shown.

and can be rapidly mutated in the absence of selective pressures.

Both ORF7a and ORF7b are Golgi-localized integral membrane proteins (31, 44, 57). The ORF7a protein has a 15-residue N-terminal signal sequence and is predicted to have an 81-residue luminal domain, a 21-residue transmembrane segment, and a 5-amino-acid cytoplasmic tail. Nelson et al. (44), and our unpublished data, demonstrate that the short cytoplasmic tail (KRKTE) serves not as an ER retrieval motif, as suggested by Fielding et al. (18), but as a dibasic ER export signal (RK]x[RK) similar to motifs responsible for ER export of Golgi-resident glycosyltransferases (19). Mutation of either the lysine at position 118 or the lysine at position 120 results in a loss of Golgi localization and a subsequent increase in colocalization with the ER marker calnexin, suggesting that the residues are critical for the ER exit of the ORF7a protein. It has been suggested that ORF7a can associate with mitochondria, the ER, and the ER-Golgi intermediate compartment after expression from cDNA (18, 67); however, we find no evidence for ORF7a colocalization with the MitoTracker dye and find that the majority of the protein colocalizes with Golgi markers (Fig. 2).

The ORF7a protein has been suggested to interact with the small glutamine-rich tetraicopeptide repeat-containing protein hSGT (17). hSGT has numerous proposed functions, including cochaperone activity (1), potential roles in cell division (72), and potential roles in apoptosis induction (71), and has been shown to interact with the parvovirus NS1 protein in the nuclei of infected cells for regulation of viral gene expression (12). The interactions between ORF7a and hSGT were mapped to the signal peptide and ectodomain (residues 1 to 96). Our results (44) suggest that the signal peptide is efficiently cleaved upon translocation of ORF7a into the ER and that the ectodomain of ORF7a resides within the ER/Golgi lumen. Since hSGT is a cytosolic protein (77), it is not clear if or how the membrane topology barrier can be overcome in order to facilitate an interaction between these proteins.

Initiation of the apoptotic cascade may result from a change in the balance of pro- and antiapoptotic host cell proteins (reviewed in reference 22). One such antiapoptotic protein, Bcl-X_L, has been shown to interact directly with the ORF7a protein (67). While we find no data to suggest that ORF7a or ORF7b localizes to mitochondria, it is possible that the ORF7a protein may interact with Bcl-X_L in the ER, prior to ORF7a trafficking to the Golgi apparatus. The interaction may lead to sequestering of Bcl-X_L in the Golgi apparatus, tipping the balance within the cell to a proapoptotic state and resulting in inhibition of protein synthesis and p38 MAPK activation. Further studies monitoring subcellular localization of Bcl-X_L in ORF7a-transfected and SARS-CoV-infected cells may provide valuable insight into any relevant interaction that ORF7a may have with Bcl-X_L during virus infection.

Programmed cell death is an evolutionarily conserved mechanism for removing extraneous, damaged, or infected cells in a systematic and regulated fashion without inducing inflammation. Several cellular organelles are capable of sensing proapoptotic signals, including the ER, lysosomes, and mitochondria (16). Although ER stress can induce apoptosis, the ER stress-induced MAPK JNK is not activated after ORF7a expression; however, p38 MAPK is activated by ORF7a expression, suggesting that the inhibition of protein synthesis and induction of apoptosis are not due to misfolded protein accumulation in the ER (31). The Golgi complex has recently been implicated in stress signaling and may play a much larger role in induction of apoptosis than previously thought (22, 39). Stress signaling and apoptotic cascades may be initiated

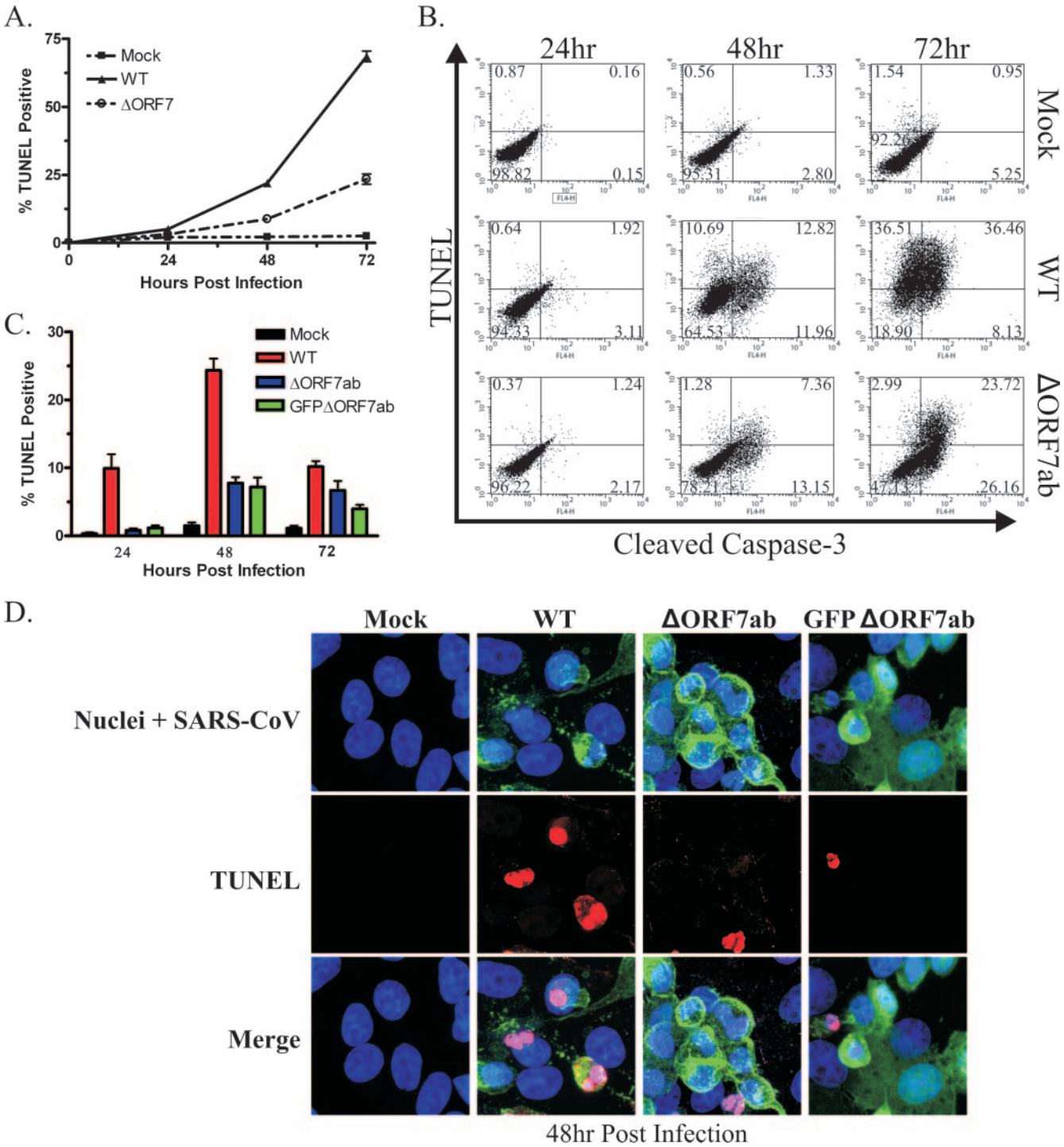

FIG. 9. Infection of Vero cells with SARS-CoV lacking gene 7 results in a significant decrease in TUNEL-positive cell populations compared to infection with wild-type virus. (A) Vero cells were mock infected or infected at an MOI of 5.0 with rSARS-CoV WT or rSARS-CoV ΔORF7ab, and cells were analyzed for late stages of apoptosis by TUNEL-FITC staining. Cells were harvested at the designated times postinfection, fixed, stained with a TUNEL-FITC labeling reaction, and analyzed by flow cytometry. All data points were determined in triplicate and graphed as mean plus standard error. The assay was repeated three times to confirm results; the data shown are from one representative experiment. (B) Vero cells were mock infected or infected at an MOI of 5.0 with rSARS-CoV WT or rSARS-CoV ΔORF7ab, and cells were analyzed for both TUNEL-FITC staining and active caspase 3 by flow cytometry. Cells were harvested at the designated times postinfection, fixed, stained with anti-active caspase 3 antibody followed by a TUNEL-FITC labeling reaction, and analyzed by flow cytometry. By 48 h, significantly fewer TUNEL-positive cells (vertical axis, left and right top quadrants) were observed in cells infected with rSARS-CoV ΔORF7ab compared to wild-type virus. Similar numbers of cells containing active caspase 3 (horizontal axis, upper and lower right quadrants), however, were detectable in cells infected with either virus. All samples were analyzed in triplicate. The data shown are from one representative sample. The percentage of cells in each quadrant is displayed. (C and D) TUNEL analysis by confocal microscopy. Vero cells grown on coverslips were either mock infected or infected with

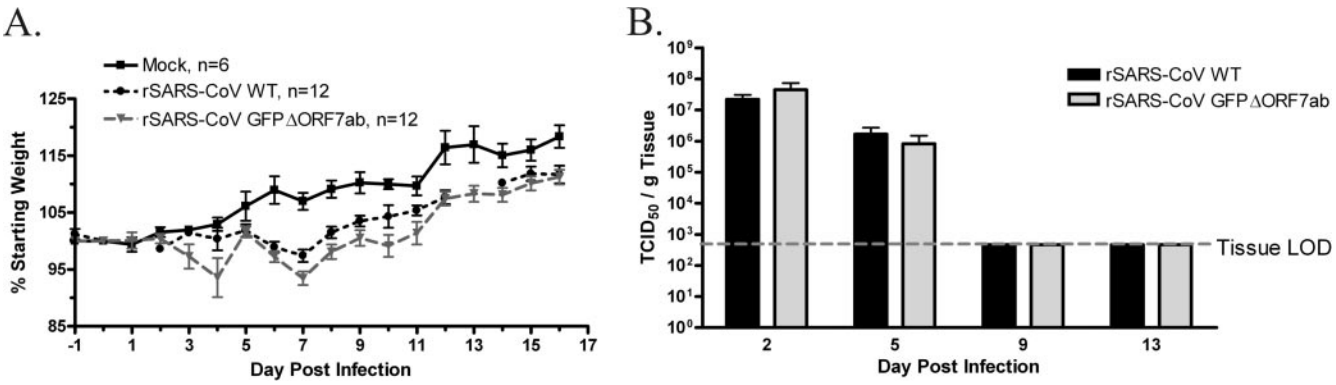

FIG. 10. Infection of golden Syrian hamsters with recombinant wild-type and gene 7 deletion viruses. Golden Syrian hamsters were inoculated intranasally with either saline or 10^3 $TCID_{50}$ of either rSARS-CoV WT or rSARS-CoV GFPΔORF7ab. (A) Individual animals were weighed, and data were normalized to animal weight on day 0. The data represent average normalized weight plus standard error. (B) Lung tissues were harvested at the indicated days postinfection, and virus load was determined by $TCID_{50}$ assay. Data represent the average titer plus standard error for six (rSARS-CoV WT) and three (rSARS-CoV GFPΔORF7ab) animals per time point.

through a complement of Golgi-localized sensory proteins. Given the high colocalization of both ORF7a and ORF7b to the Golgi complex, it is possible that the accessory proteins contribute to the apoptotic cascade via Golgi-dependent mechanisms. The absence of ORF7a and ORF7b in virus-infected cells may result in skewing of proapoptotic signals from different subcellular organelles, resulting in a different apoptotic phenotype than in cells infected with wild-type virus. The decrease in TUNEL-positive cells observed with gene 7 deletion viruses may be due to decreased activation of one or both of the major endonucleases responsible for DNA degradation in apoptotic cells: the cytoplasmic endonuclease CAD/DFF40 or the mitochondrial activated endonuclease G (reviewed in reference 70). It has been demonstrated that cells can undergo apoptosis with caspase activation in the absence of DNA fragmentation (11, 61, 82, 83), suggesting that the two activities are not mutually inclusive and may be activated via separate biochemical stimuli.

Necrosis has been observed in tissues from SARS-CoV-infected patients, and cDNA expression of the ORF3b protein in Vero cells has been shown to induce necrosis (29). Although DNA fragmentation can occur in necrotic cells, it is random and appears as a "smear" in agarose gels compared to the ordered nucleosomal laddering observed in apoptotic cells (83). The DNA fragmentation observed in necrotic cells can sometimes be detected by TUNEL staining. It is possible that infection with wild-type virus, encoding both gene 7 accessory proteins, yields a population of necrotic cells detectable by TUNEL staining that is not observed upon infection with gene 7 deletion viruses. At 48 and 72 h postinfection, a TUNEL-positive and caspase 3-negative population exists (Fig. 9B) in cells infected with wild-type virus that is not present in cells infected with gene 7 deletion viruses. These cells may represent a population in late stages of apoptosis or, conversely, may represent a population of necrotic cells. While neither ORF7a nor ORF7b has been reported to induce necrosis upon cDNA transfection to date, it will be important to readdress this topic in light of our data.

Death of infected cells can be induced either directly by specific viral proteins or indirectly as a consequence of the functional effects of the viral protein on the cell. It has been proposed that some viruses take advantage of apoptotic responses to facilitate invasion and/or enhance pathogenesis (8). Examples of proapoptotic viral proteins include adenovirus E1A and E4orf4 (2); human immunodeficiency virus type 1 Tat, Nef, Vpr, and gp120 (54); the chicken anemia virus protein apoptin (50); dengue virus M protein (3); and the influenza A virus protein PB1-F2 (7). Clear roles for the proapoptotic functions of these proteins are not well defined; however, it is likely that the cell death function of each aids in promoting viral spread, replication, or immune evasion in vivo (8, 32, 74).

Deletion of gene 7 does not alter SARS-CoV infection and replication in the lungs of BALB/c mice (79). It is possible that ORF7a and ORF7b may be dispensable for replication in the current SARS-CoV animal models. ORF7a and ORF7b may play functional roles in human infection, as the time frame for infection is significantly prolonged and disease is much more pronounced compared to those in the available small animal models or in virus transmission (62). The gene 7 coding region is also highly conserved in bat SARS-CoV isolates, suggesting a potential role for the gene products in bat infection (37). Analyzing infection with gene 7 deletion viruses in animal

rSARS-CoV WT, rSARS-CoV GFPΔORF7ab, or rSARS-CoV ΔORF7ab at an MOI of 5.0. The cells were fixed at 24, 48, and 72 h postinfection and immunostained with a pool of mouse anti-SARS-CoV MAbs (green). Nuclei were counterstained with TO-PRO-3 nuclear stain (blue). Cells were subsequently TUNEL labeled using a TUNEL-TMR labeling kit (red) and analyzed by confocal microscopy. (C) More than 1,000 total cells were counted from three coverslips from each virus infection at each time point, and the percentage of TUNEL-positive cells was calculated and graphed as mean plus standard error. Quantified TUNEL data demonstrated a significant reduction in adherent TUNEL-positive cells at all time points in both gene 7 deletion viruses compared to wild-type virus. (D) Representative images from cells at 48 h postinfection. Significantly more SARS-CoV antigen-positive cells were TUNEL positive in rSARS-CoV WT-infected cells than in cells infected with either gene 7 deletion virus.

models that display more pronounced disease, such as Stat1-deficient mice (23), human transgenic ACE2 mice (43, 69), or aged mice (52), may also provide valuable information on potential roles for ORF7a and/or ORF7b in SARS-CoV-induced disease.

Further animal studies will be needed to evaluate the function of the ORF7a and ORF7b proteins in modulation of the immune response and overall role in the pathogenesis of SARS-CoV infection, since the induction of apoptosis can have profound effects on the immune system and the immune response to a viral pathogen. Macrophages are key players in the clearance of apoptotic cells and respond differently to cells undergoing various forms of cell death (20, 32). The apoptotic alterations observed in gene 7 deletion SARS-CoV-infected cells in vitro may translate to altered recognition of apoptotic cells in SARS-CoV-infected animals and subsequently may result in altered immune responses to the virus. Clearly, additional extensive studies of virus pathogenesis and immune response are needed to adequately address this aspect of virus infection.

ACKNOWLEDGMENTS

We thank all the members of the Pekosz laboratory for insightful discussions and comments. We acknowledge and thank Ralph Baric, University of North Carolina, for generously providing the recombinant SARS-CoV used in this study. We also acknowledge the Molecular Microbiology Imaging Facility for help with microscopy.

This study was supported by U54 AI057160, the Markey Pathway (S.R.S.), T32 HL07317 (S.R.S.), and AI059328 (A.P.).

REFERENCES

1. **Angeletti, P. C., D. Walker, and A. T. Panganiban.** 2002. Small glutamine-rich protein/viral protein U-binding protein is a novel cochaperone that affects heat shock protein 70 activity. Cell Stress Chaperones **7:**258–268.
2. **Branton, P. E., and D. E. Roopchand.** 2001. The role of adenovirus E4orf4 protein in viral replication and cell killing. Oncogene **20:**7855–7865.
3. **Catteau, A., O. Kalinina, M. C. Wagner, V. Deubel, M. P. Courageot, and P. Despres.** 2003. Dengue virus M protein contains a proapoptotic sequence referred to as ApoptoM. J Gen. Virol. **84:**2781–2793.
4. **Centers for Disease Control and Prevention.** 2003. Revised U.S. surveillance case definition for severe acute respiratory syndrome (SARS) and update on SARS cases—United States and worldwide, December 2003. Morb. Mortal. Wkly. Rep. **52:**1202–1206.
5. **Chan, W. S., C. Wu, S. C. Chow, T. Cheung, K. F. To, W. K. Leung, P. K. Chan, K. C. Lee, H. K. Ng, D. M. Au, and A. W. Lo.** 2005. Coronaviral hypothetical and structural proteins were found in the intestinal surface enterocytes and pneumocytes of severe acute respiratory syndrome (SARS). Modern Pathol. **18:**1432–1439.
6. **Chau, T. N., K. C. Lee, H. Yao, T. Y. Tsang, T. C. Chow, Y. C. Yeung, K. W. Choi, Y. K. Tso, T. Lau, S. T. Lai, and C. L. Lai.** 2004. SARS-associated viral hepatitis caused by a novel coronavirus: report of three cases. Hepatology **39:**302–310.
7. **Chen, W., P. A. Calvo, D. Malide, J. Gibbs, U. Schubert, I. Bacik, S. Basta, R. O'Neill, J. Schickli, P. Palese, P. Henklein, J. R. Bennink, and J. W. Yewdell.** 2001. A novel influenza A virus mitochondrial protein that induces cell death. Nat. Med. **7:**1306–1312.
8. **Chen, Y.-B., Y. Fannjiang, and J. M. Hardwick.** 2004. Cell death in viral infections, p. 435–460. *In* R. A. Lockshin (ed.), When cells die II. John Wiley & Sons, New York, NY.
9. **Chen, Y. Y., B. Shuang, Y. X. Tan, M. J. Meng, P. Han, X. N. Mo, Q. S. Song, X. Y. Qiu, X. Luo, Q. N. Gan, X. Zhang, Y. Zheng, S. A. Liu, X. N. Wang, N. S. Zhong, and D. L. Ma.** 2005. The protein X4 of severe acute respiratory syndrome-associated coronavirus is expressed on both virus-infected cells and lung tissue of severe acute respiratory syndrome patients and inhibits growth of Balb/c 3T3 cell line. Chin. Med. J. **118:**267–274.
10. **Chow, K. Y., Y. S. Yeung, C. C. Hon, F. Zeng, K. M. Law, and F. C. Leung.** 2005. Adenovirus-mediated expression of the C-terminal domain of SARS-CoV spike protein is sufficient to induce apoptosis in Vero E6 cells. FEBS Lett. **579:**6699–6704.
11. **Collins, J. A., C. A. Schandi, K. K. Young, J. Vesely, and M. C. Willingham.** 1997. Major DNA fragmentation is a late event in apoptosis. J. Histochem. Cytochem. **45:**923–934.
12. **Cziepluch, C., S. Lampel, A. Grewenig, C. Grund, P. Lichter, and J. Rommelaere.** 2000. H-1 parvovirus-associated replication bodies: a distinct virus-induced nuclear structure. J. Virol. **74:**4807–4815.
13. **de Haan, C. A. M., P. S. Masters, X. Shen, S. Weiss, and P. J. M. Rottier.** 2002. The group-specific murine coronavirus genes are not essential, but their deletion, by reverse genetics, is attenuating in the natural host. Virology **296:**177–189.
14. **Ding, Y., L. He, Q. Zhang, Z. Huang, X. Che, J. Hou, H. Wang, H. Shen, L. Qiu, Z. Li, J. Geng, J. Cai, H. Han, X. Li, W. Kang, D. Weng, P. Liang, and S. Jiang.** 2004. Organ distribution of severe acute respiratory syndrome (SARS) associated coronavirus (SARS-CoV) in SARS patients: implications for pathogenesis and virus transmission pathways. J. Pathol. **203:**622–630.
15. **Ding, Y., H. Wang, H. Shen, Z. Li, J. Geng, H. Han, J. Cai, X. Li, W. Kang, D. Weng, Y. Lu, D. Wu, L. He, and K. Yao.** 2003. The clinical pathology of severe acute respiratory syndrome (SARS): a report from China. J. Pathol. **200:**282–289.
16. **Ferri, K. F., and G. Kroemer.** 2001. Organelle-specific initiation of cell death pathways. Nat. Cell Biol. **3:**E255–E263.
17. **Fielding, B. C., V. Gunalan, T. H. P. Tan, C.-F. Chou, S. Shen, S. Khan, S. G. Lim, W. Hong, and Y.-J. Tan.** 2006. Severe acute respiratory syndrome coronavirus protein 7a interacts with hSGT. Biochem. Biophys. Res. Commun. **343:**1201–1208.
18. **Fielding, B. C., Y.-J. Tan, S. Shuo, T. H. P. Tan, E.-E. Ooi, S. G. Lim, W. Hong, and P.-Y. Goh.** 2004. Characterization of a unique group-specific protein (U122) of the severe acute respiratory syndrome coronavirus. J. Virol. **78:**7311–7318.
19. **Giraudo, C. G., and H. J. Maccioni.** 2003. Endoplasmic reticulum export of glycosyltransferases depends on interaction of a cytoplasmic dibasic motif with Sar1. Mol. Biol. Cell **14:**3753–3766.
20. **Gregory, C. D., and A. Devitt.** 2004. The macrophage and the apoptotic cell: an innate immune interaction viewed simplistically? Immunology **113:**1–14.
21. **Gu, J., and C. Korteweg.** 2007. Pathology and pathogenesis of severe acute respiratory syndrome. Am. J. Pathol. **170:**1136–1147.
22. **Hicks, S. W., and C. E. Machamer.** 2005. Golgi structure in stress sensing and apoptosis. Biochim. Biophys. Acta **1744:**406–414.
23. **Hogan, R. J., G. Gao, T. Rowe, P. Bell, D. Flieder, J. Paragas, G. P. Kobinger, N. A. Wivel, R. G. Crystal, J. Boyer, H. Feldmann, T. G. Voss, and J. M. Wilson.** 2004. Resolution of primary severe acute respiratory syndrome-associated coronavirus infection requires Stat1. J. Virol. **78:**11416–11421.
24. **Huang, C., N. Ito, C.-T. K. Tseng, and S. Makino.** 2006. Severe acute respiratory syndrome coronavirus 7a accessory protein is a viral structural protein. J. Virol. **80:**7287–7294.
25. **Huang, C., K. Narayanan, N. Ito, C. J. Peters, and S. Makino.** 2006. Severe acute respiratory syndrome coronavirus 3a protein is released in membranous structures from 3a protein-expressing cells and infected cells. J. Virol. **80:**210–217.
26. **Hwang, D. M., D. W. Chamberlain, S. M. Poutanen, D. E. Low, S. L. Asa, and J. Butany.** 2005. Pulmonary pathology of severe acute respiratory syndrome in Toronto. Mod. Pathol. **18:**1–10.
27. **Ito, N., E. C. Mossel, K. Narayanan, V. L. Popov, C. Huang, T. Inoue, C. J. Peters, and S. Makino.** 2005. Severe acute respiratory syndrome coronavirus 3a protein is a viral structural protein. J. Virol. **79:**3182–3186.
28. **Kanzawa, N., K. Nishigaki, T. Hayashi, Y. Ishii, S. Furukawa, A. Niiro, F. Yasui, M. Kohara, K. Morita, and K. Matsushima.** 2006. Augmentation of chemokine production by severe acute respiratory syndrome coronavirus 3a/X1 and 7a/X4 proteins through NF-κB activation. FEBS Lett. **580:**6807–6812.
29. **Khan, S., B. C. Fielding, T. H. P. Tan, C.-F. Chou, S. Shen, S. G. Lim, W. Hong, and Y.-J. Tan.** 2006. Over-expression of severe acute respiratory syndrome coronavirus 3b protein induces both apoptosis and necrosis in Vero E6 cells. Virus Res. **122:**20–27.
30. **Kopecky-Bromberg, S. A., L. Martinez-Sobrido, M. Frieman, R. A. Baric, and P. Palese.** 2007. Severe acute respiratory syndrome coronavirus open reading frame (ORF) 3b, ORF 6, and nucleocapsid proteins function as interferon antagonists. J. Virol. **81:**548–557.
31. **Kopecky-Bromberg, S. A., L. Martinez-Sobrido, and P. Palese.** 2006. 7a protein of severe acute respiratory syndrome coronavirus inhibits cellular protein synthesis and activates p38 mitogen-activated protein kinase. J. Virol. **80:**785–793.
32. **Krysko, D., K. D'Herde, and P. Vandenabeele.** 2006. Clearance of apoptotic and necrotic cells and its immunological consequences. Apoptosis **11:**1709–1726.
33. **Lai, C. W., Z. R. Chan, D. G. Yang, W. H. Lo, Y. K. Lai, M. D. Chang, and Y. C. Hu.** 2006. Accelerated induction of apoptosis in insect cells by baculovirus-expressed SARS-CoV membrane protein. FEBS Lett. **580:**3829–3834.
34. **Lang, Z. W., L. J. Zhang, S. J. Zhang, X. Meng, J. Q. Li, C. Z. Song, L. Sun, Y. S. Zhou, and D. E. Dwyer.** 2003. A clinicopathological study of three cases of severe acute respiratory syndrome (SARS). Pathology **35:**526–531.
35. **Lau, Y. L., and J. S. M. Peiris.** 2005. Pathogenesis of severe acute respiratory syndrome. Curr. Opin. Immunol. **17:**404–410.

36. **Law, P. T. W., C.-H. Wong, T. C. C. Au, C.-P. Chuck, S.-K. Kong, P. K. S. Chan, K.-F. To, A. W. I. Lo, J. Y. W. Chan, Y.-K. Suen, H. Y. E. Chan, K.-P. Fung, M. M. Y. Waye, J. J. Y. Sung, Y. M. D. Lo, and S. K. W. Tsui.** 2005. The 3a protein of severe acute respiratory syndrome-associated coronavirus induces apoptosis in Vero E6 cells. J. Gen. Virol. **86:**1921–1930.
37. **Li, W., Z. Shi, M. Yu, W. Ren, C. Smith, J. H. Epstein, H. Wang, G. Crameri, Z. Hu, H. Zhang, J. Zhang, J. McEachern, H. Field, P. Daszak, B. T. Eaton, S. Zhang, and L.-F. Wang.** 2005. Bats are natural reservoirs of SARS-like coronaviruses. Science **310:**676–679.
38. **Lin, C. W., K. H. Lin, T. H. Hsieh, S. Y. Shiu, and J. Y. Li.** 2006. Severe acute respiratory syndrome coronavirus 3C-like protease-induced apoptosis. FEMS Immunol. Med. Microbiol. **46:**375–380.
39. **Maag, R. S., S. W. Hicks, and C. E. Machamer.** 2003. Death from within: apoptosis and the secretory pathway. Curr. Opin. Cell Biol. **15:**456–461.
40. **Marra, M. A., S. J. M. Jones, C. R. Astell, R. A. Holt, A. Brooks-Wilson, Y. S. N. Butterfield, J. Khattra, J. K. Asano, S. A. Barber, S. Y. Chan, A. Cloutier, S. M. Coughlin, D. Freeman, N. Girn, O. L. Griffith, S. R. Leach, M. Mayo, H. McDonald, S. B. Montgomery, P. K. Pandoh, A. S. Petrescu, A. G. Robertson, J. E. Schein, A. Siddiqui, D. E. Smailus, J. M. Stott, G. S. Yang, F. Plummer, A. Andonov, H. Artsob, N. Bastien, K. Bernard, T. F. Booth, D. Bowness, M. Czub, M. Drebot, L. Fernando, R. Flick, M. Garbutt, M. Gray, A. Grolla, S. Jones, H. Feldmann, A. Meyers, A. Kabani, Y. Li, S. Normand, U. Stroher, G. A. Tipples, S. Tyler, R. Vogrig, D. Ward, B. Watson, R. C. Brunham, M. Krajden, M. Petric, D. M. Skowronski, C. Upton, and R. L. Roper.** 2003. The genome sequence of the SARS-associated coronavirus. Science **300:**1399–1404.
41. **McCown, M., M. S. Diamond, and A. Pekosz.** 2003. The utility of siRNA transcripts produced by RNA polymerase i in down regulating viral gene expression and replication of negative- and positive-strand RNA viruses. Virology **313:**514–524.
42. **McCown, M. F., and A. Pekosz.** 2005. The influenza A virus M2 cytoplasmic tail is required for infectious virus production and efficient genome packaging. J. Virol. **79:**3595–3605.
43. **McCray, P. B., Jr., L. Pewe, C. Wohlford-Lenane, M. Hickey, L. Manzel, L. Shi, J. Netland, H. P. Jia, C. Halabi, C. D. Sigmund, D. K. Meyerholz, P. Kirby, D. C. Look, and S. Perlman.** 2007. Lethal infection of K18-hACE2 mice infected with severe acute respiratory syndrome coronavirus. J. Virol. **81:**813–821.
44. **Nelson, C. A., A. Pekosz, C. A. Lee, M. S. Diamond, and D. H. Fremont.** 2005. Structure and intracellular targeting of the SARS-coronavirus Orf7a accessory protein. Structure (Cambridge) **13:**75–85.
45. **Ortego, J., I. Sola, F. Almazan, J. E. Ceriani, C. Riquelme, M. Balasch, J. Plana, and L. Enjuanes.** 2003. Transmissible gastroenteritis coronavirus gene 7 is not essential but influences in vivo virus replication and virulence. Virology **308:**13–22.
46. **Pekosz, A., C. Griot, N. Nathanson, and F. Gonzalez-Scarano.** 1995. Tropism of bunyaviruses: evidence for a G1 glycoprotein-mediated entry pathway common to the California serogroup. Virology **214:**339–348.
47. **Pekosz, A., and R. A. Lamb.** 1997. The CM2 protein of influenza C virus is an oligomeric integral membrane glycoprotein structurally analogous to influenza A virus M2 and influenza B virus NB proteins. Virology **237:**439–451.
48. **Pekosz, A., J. Phillips, D. Pleasure, D. Merry, and F. Gonzalez-Scarano.** 1996. Induction of apoptosis by La Crosse virus infection and role of neuronal differentiation and human bcl-2 expression in its prevention. J. Virol. **70:**5329–5335.
49. **Pekosz, A., S. R. Schaecher, M. S. Diamond, D. H. Fremont, A. C. Sims, and R. S. Baric.** 2006. Structure, expression, and intracellular localization of the SARS-CoV accessory proteins 7a and 7b. Adv. Exp. Med. Biol. **581:**115–120.
50. **Pietersen, A., and H. M. Noteborn.** 2000. Apoptin. Adv. Exp. Med. Biol. **465:**153–161.
51. **Potten, C. S., and J. Wilson.** 2004. Apoptosis: the life and death of cells. Cambridge University Press, New York, NY.
52. **Roberts, A., C. Paddock, L. Vogel, E. Butler, S. Zaki, and K. Subbarao.** 2005. Aged BALB/c mice as a model for increased severity of severe acute respiratory syndrome in elderly humans. J. Virol. **79:**5833–5838.
53. **Roberts, A., L. Vogel, J. Guarner, N. Hayes, B. Murphy, S. Zaki, and K. Subbarao.** 2005. Severe acute respiratory syndrome coronavirus infection of golden Syrian hamsters. J. Virol. **79:**503–511.
54. **Roshal, M., Y. Zhu, and V. Planelles.** 2001. Apoptosis in AIDS. Apoptosis **6:**103–116.
55. **Rota, P. A., M. S. Oberste, S. S. Monroe, W. A. Nix, R. Campagnoli, J. P. Icenogle, S. Penaranda, B. Bankamp, K. Maher, M.-h. Chen, S. Tong, A. Tamin, L. Lowe, M. Frace, J. L. DeRisi, Q. Chen, D. Wang, D. D. Erdman, T. C. T. Peret, C. Burns, T. G. Ksiazek, P. E. Rollin, A. Sanchez, S. Liffick, B. Holloway, J. Limor, K. McCaustland, M. Olsen-Rasmussen, R. Fouchier, S. Gunther, A. D. M. E. Osterhaus, C. Drosten, M. A. Pallansch, L. J. Anderson, and W. J. Bellini.** 2003. Characterization of a novel coronavirus associated with severe acute respiratory syndrome. Science **300:**1394–1399.
56. **Rowe, R. K., S. L. Brody, and A. Pekosz.** 2004. Differentiated cultures of primary hamster tracheal airway epithelial cells. In Vitro Cell Dev. Biol. Anim. **40:**303–311.
57. **Schaecher, S. R., J. M. Mackenzie, and A. Pekosz.** 2007. The ORF7b protein of severe acute respiratory syndrome coronavirus (SARS-CoV) is expressed in virus-infected cells and incorporated into SARS-CoV particles. J. Virol. **81:**718–731.
58. **Shao, R. G., T. Shimizu, and Y. Pommier.** 1996. Brefeldin A is a potent inducer of apoptosis in human cancer cells independently of p53. Exp. Cell Res. **227:**190–196.
59. **Shen, S., P. S. Lin, Y. C. Chao, A. Zhang, X. Yang, S. G. Lim, W. Hong, and Y. J. Tan.** 2005. The severe acute respiratory syndrome coronavirus 3a is a novel structural protein. Biochem. Biophys. Res. Commun. **330:**286–292.
60. **Sims, A. C., R. S. Baric, B. Yount, S. E. Burkett, P. L. Collins, and R. J. Pickles.** 2005. Severe acute respiratory syndrome coronavirus infection of human ciliated airway epithelia: role of ciliated cells in viral spread in the conducting airways of the lungs. J. Virol. **79:**15511–15524.
61. **Solovyan, V. T., Z. A. Bezvenyuk, A. Salminen, C. A. Austin, and M. J. Courtney.** 2002. The role of topoisomerase II in the excision of DNA loop domains during apoptosis. J. Biol. Chem. **277:**21458–21467.
62. **Subbarao, K., and A. Roberts.** 2006. Is there an ideal animal model for SARS? Trends Microbiol. **14:**299–303.
63. **Surjit, M., B. Liu, S. Jameel, V. T. Chow, and S. K. Lal.** 2004. The SARS coronavirus nucleocapsid protein induces actin reorganization and apoptosis in COS-1 cells in the absence of growth factors. Biochem. J. **383:**13–18.
64. **Takeda, M., A. Pekosz, K. Shuck, L. H. Pinto, and R. A. Lamb.** 2002. Influenza A virus M_2 ion channel activity is essential for efficient replication in tissue culture. J. Virol. **76:**1391–1399.
65. **Takizawa, T., S. Matsukawa, Y. Higuchi, S. Nakamura, Y. Nakanishi, and R. Fukuda.** 1993. Induction of programmed cell death (apoptosis) by influenza virus infection in tissue culture cells. J. Gen. Virol. **74:**2347–2355.
66. **Tan, Y.-J., B. C. Fielding, P.-Y. Goh, S. Shen, T. H. P. Tan, S. G. Lim, and W. Hong.** 2004. Overexpression of 7a, a protein specifically encoded by the severe acute respiratory syndrome coronavirus, induces apoptosis via a caspase-Dependent pathway. J. Virol. **78:**14043–14047.
67. **Tan, Y.-X., T. H. P. Tan, M. J. R. Lee, P.-Y. Tham, V. Gunalan, J. Druce, C. Birch, M. Catton, N. Y. Fu, V. C. Yu, and Y.-J. Tan.** 2007. Induction of apoptosis by the severe acute respiratory syndrome coronavirus 7a protein is dependent on its interaction with the Bcl-X_L protein. J. Virol. **81:**6346–6355.
68. **Thiel, V., K. A. Ivanov, A. Putics, T. Hertzig, B. Schelle, S. Bayer, B. Weissbrich, E. J. Snijder, H. Rabenau, H. W. Doerr, A. E. Gorbalenya, and J. Ziebuhr.** 2003. Mechanisms and enzymes involved in SARS coronavirus genome expression. J. Gen. Virol. **84:**2305–2315.
69. **Tseng, C.-T. K., C. Huang, P. Newman, N. Wang, K. Narayanan, D. M. Watts, S. Makino, M. M. Packard, S. R. Zaki, T.-S. Chan, and C. J. Peters.** 2007. Severe acute respiratory syndrome coronavirus infection of mice transgenic for the human angiotensin-converting enzyme 2 virus receptor. J. Virol. **81:**1162–1173.
70. **Van Lancker, J. L.** 2006. Apoptosis, genomic integrity, and cancer. Jones and Bartlett Publishers, Sudbury, MA.
71. **Wang, H., H. Shen, Y. Wang, Z. Li, H. Yin, H. Zong, J. Jiang, and J. Gu.** 2005. Overexpression of small glutamine-rich TPR-containing protein promotes apoptosis in 7721 cells. FEBS Lett. **579:**1279–1284.
72. **Winnefeld, M., J. Rommelaere, and C. Cziepluch.** 2004. The human small glutamine-rich TPR-containing protein is required for progress through cell division. Exp. Cell Res. **293:**43–57.
73. **Wong, S. L., Y. Chen, C. M. Chan, C. S. Chan, P. K. Chan, Y. L. Chui, K. P. Fung, M. M. Waye, S. K. Tsui, and H. Y. Chan.** 2005. In vivo functional characterization of the SARS-coronavirus 3a protein in Drosophila. Biochem. Biophys. Res. Commun. **337:**720–729.
74. **Xu, W., A. Roos, M. R. Daha, and C. van Kooten.** 2006. Dendritic cell and macrophage subsets in the handling of dying cells. Immunobiology **211:**567–575.
75. **Yamashita, M., M. Yamate, G. M. Li, and K. Ikuta.** 2005. Susceptibility of human and rat neural cell lines to infection by SARS-coronavirus. Biochem. Biophys. Res. Commun. **334:**79–85.
76. **Yang, Y., Z. Xiong, S. Zhang, Y. Yan, J. Nguyen, B. Ng, H. Lu, J. Brendese, F. Yang, H. Wang, and X. F. Yang.** 2005. Bcl-xL inhibits T-cell apoptosis induced by expression of SARS coronavirus E protein in the absence of growth factors. Biochem. J. **392:**135–143.
77. **Yin, H., H. Wang, H. Zong, X. Chen, Y. Wang, X. Yun, Y. Wu, J. Wang, and J. Gu.** 2006. SGT, a Hsp90beta binding partner, is accumulated in the nucleus during cell apoptosis. Biochem. Biophys. Res. Commun. **343:**1153–1158.
78. **Yount, B., K. M. Curtis, E. A. Fritz, L. E. Hensley, P. B. Jahrling, E. Prentice, M. R. Denison, T. W. Geisbert, and R. S. Baric.** 2003. Reverse genetics with a full-length infectious cDNA of severe acute respiratory syndrome coronavirus. Proc. Natl. Acad. Sci. USA **100:**12995–13000.
79. **Yount, B., R. S. Roberts, A. C. Sims, D. Deming, M. B. Frieman, J. Sparks, M. R. Denison, N. Davis, and R. S. Baric.** 2005. Severe acute respiratory syndrome coronavirus group-specific open reading frames encode nonessential functions for replication in cell cultures and mice. J. Virol. **79:**14909–14922.
80. **Yuan, X., Y. Shan, Z. Zhao, J. Chen, and Y. Cong.** 2005. G0/G1 arrest and apoptosis induced by SARS-CoV 3b protein in transfected cells. Virol. J. **2:**66.

81. **Yuan, X., J. Wu, Y. Shan, Z. Yao, B. Dong, B. Chen, Z. Zhao, S. Wang, J. Chen, and Y. Cong.** 2006. SARS coronavirus 7a protein blocks cell cycle progression at G0/G1 phase via the cyclin D3/pRb pathway. Virology **346:** 74–85.
82. **Yuste, V. J., J. R. Bayascas, N. Llecha, I. Sanchez-Lopez, J. Boix, and J. X. Comella.** 2001. The absence of oligonucleosomal DNA fragmentation during apoptosis of IMR-5 neuroblastoma cells: disappearance of the caspase-activated DNase. J. Biol. Chem. **276:**22323–22331.
83. **Zhang, J., and M. Xu.** 2002. Apoptotic DNA fragmentation and tissue homeostasis. Trends Cell Biol. **12:**84–89.
84. **Zhao, G., S. Q. Shi, Y. Yang, and J. P. Peng.** 2006. M and N proteins of SARS coronavirus induce apoptosis in HPF cells. Cell Biol. Toxicol. **22:**313–322.